frontiers in Nanotechnology

ORIGINAL RESEARCH
published: 13 April 2021
doi: 10.3389/fnano.2021.635929

Ultraviolet-Filtering Luminescent Transparent Coatings for High-Performance PTB7-Th: ITIC–Based Organic Solar Cells

Joana Farinhas[1†], Sandra F. H. Correia[2†], Lianshe Fu[2], Alexandre M. P. Botas[2], Paulo S. André[1,3], Rute A. S. Ferreira[2] and Ana Charas[1]**

[1]Instituto de Telecomunicações, Instituto Superior Técnico, Lisboa, Portugal, [2]Department of Physics and CICECO—Aveiro Institute of Materials, University of Aveiro, Aveiro, Portugal, [3]Department of Electric and Computer Engineering Instituto Superior Técnico, Universidade de Lisboa, Lisbon, Portugal

OPEN ACCESS

Edited by:
Karthik Ramasamy,
UbiQD, Inc., United States

Reviewed by:
Nikolay S. Makarov,
UbiQD, Inc., United States
Pravin Shinde,
University of Alabama, United States
Soubantika Palchoudhury,
University of Tennessee at Chattanooga, United States

***Correspondence:**
Rute A. S. Ferreira
rferreira@ua.pt
Ana Charas
ana.charas@lx.it.pt

[†]These authors have contributed equally to this work

Specialty section:
This article was submitted to Nanotechnology for Energy Applications, a section of the journal Frontiers in Nanotechnology

Received: 30 November 2020
Accepted: 09 February 2021
Published: 13 April 2021

Citation:
Farinhas J, Correia SFH, Fu L, Botas AMP, André PS, Ferreira RAS and Charas A (2021) Ultraviolet-Filtering Luminescent Transparent Coatings for High-Performance PTB7-Th:ITIC–Based Organic Solar Cells. Front. Nanotechnol. 3:635929. doi: 10.3389/fnano.2021.635929

Photovoltaic (PV) devices based on organic heterojunctions have recently achieved remarkable power conversion efficiency (PCE) values. However, photodegradation is often a cause of dramatic drops in device performance. The use of ultraviolet (UV)-absorbing luminescent downshifting (LDS) layers can be a mitigation strategy to simultaneously filter UV radiation reaching the device and reemit it with lower energy in the visible spectral range, matching the maximum spectral response of the PV cells and thus enabling the increase of the photocurrent generated by the cell. In this work, we report the use of a Eu^{3+}-doped siliceous-based organic–inorganic hybrid as a coating on organic solar cells based on the PTB7-Th:ITIC bulk heterojunction with the purpose of increasing their performance. We found that the applied coatings yield a PCE enhancement of ~22% (from 3.1 to 3.8%) in solar cells with spin-coated layers, compared with the bare solar cells, which is among the highest performance enhancements induced by plastic luminescent coatings.

Keywords: luminescent downshifting, UV filters, organic solar cells, photodegradation, organic-inorganic hybrids

INTRODUCTION

Photovoltaic (PV) solar cells based on solution-processed organic semiconductors, either polymers or small molecules, arranged in bulk heterojunctions (BHJ) as the photoactive layer, have recently exhibited remarkable performance in small-area devices, proving great promise as competitors of their well-established inorganic counterparts. Furthermore, organic photovoltaic (OPV) technology is especially attractive because low-cost deposition methods, such as roll-to-roll printing, can be employed in its manufacture, and semitransparent and light-weight modules can be fabricated over glass or curved plastic substrates. This makes OPV technology particularly advantageous for building integration, as windows and facades generate electricity while simultaneously protecting against heat and UV irradiation. Today, most efficient OPV solar cells, exhibiting efficiencies above 17%, contain active layers of ternary blends of the polymer donor PBDB-T-2F, the fullerene [6,6]-phenyl-C71-butyric acid methyl ester ($PC_{71}BM$), and the non-fullerene acceptor Y6 (Lin et al., 2019). A comprehensive analysis on the progress of OPV solar cells and their performance is given by Xu and coworkers in a recent review (Xu et al., 2020). Y6 belongs to a new class of non-fullerene acceptors (NFAs) based on a central core of fused aromatic rings linked to electron-deficient end

units, whose molecular design enables surpassing the drawbacks of the standard fullerene acceptors, $PC_{60}BM$ and $PC_{70}BM$, by exhibiting broader absorption of the solar radiation. Nevertheless, OPVs still face a few challenges in making a successful pathway into large-scale commercialization. Several studies have demonstrated a noteworthy photoinduced degradation of device parameters even in the absence of oxygen and moisture, which is particularly different from that of crystalline silicon-based counterparts, which are relatively stable under sunlight. In fact, device efficiency can drop by 10–50% even in well-encapsulated devices, which is a serious drawback considering the moderate starting PCE values of OPVs (Peters et al., 2012; Liu et al., 2017; Mateker and Mcgehee, 2017). Ways to eliminate or minimize such intrinsic degradation (it contrasts with extrinsic degradation that involves oxygen and moisture from the atmosphere) are still little understood and can depend on the materials forming the BHJ and/or specificities of their interactions in the BHJ. In solar cells with polymer:PC_xBM (x = 60, 70) BHJs, photo-dimerization of the fullerene acceptor (Distler et al., 2014; Heumueller et al., 2016) and light-induced defect states in the polymer (Peters et al., 2012; Distler et al., 2014; Kong et al., 2014; Heumueller et al., 2016) have been related to lower currents and voltages. In addition, photoinduced burn-in was also correlated with less densely packed BHJ morphologies (Heumueller et al., 2014; Heumueller et al., 2015). As for cells with NFAs, superior photoinduced intrinsic degradation was documented for devices with the efficient ITIC acceptor than for $PC_{71}BM$-based counterparts (Doumon et al., 2019). The authors identified that the fill factor (FF) is the most affected parameter and correlated it with changes in charge carriers mobilities upon light exposure. Other authors determined that photochemical reactions on such systems could ultimately create recombination centers and negatively affect charge transport within the BHJ (Upama et al., 2017). One strategy to prevent intrinsic photoinduced device degradation consists of reducing the UV portion of the incident radiation in the device. To test this possibility, Cha et al. used radiation without UV to illuminate encapsulated devices with an efficient polymer:NFA BHJ made of PffBT4T-2OD:EH-IDTBR, and found superior performance stability (Cha et al., 2017). Other proposals used UV longpass filters with different cutoff wavelengths to illuminate OPV cells based on PTB7-Th:PCBM blends and obtained significant improvements in both open-circuit voltage (V_{OC}) and short-circuit current density (J_{SC}) for filters cutting up to 400 nm (Liu et al., 2017).

A major problem limiting the conversion efficiency of PV cells is their insensitivity to the full solar spectrum. The nonabsorption losses can be minimized using luminescent materials as spectral converters, involving the incorporation of a passive luminescent layer on PV cells. In this case, the active materials of the solar cells present a lower response in the UV spectral region (300–400 nm) than that of the visible one (600–750 nm). Thus, adding a luminescent layer able to absorb the incident UV photons (high absorption coefficient, see **Supplementary Figure S3**) and convert them to visible ones (e.g., ~615 nm) should be beneficial, by increasing the number of available visible photons for absorption by the solar cell, increasing the generated photocurrent, and, consequently, inducing an enhancement in the solar cells' performance. Lanthanide (Ln^{3+})-based complexes (e.g., Ln = Eu and Tb) absorb high-energy UV photons and efficiently emit lower-energy visible photons, thereby simultaneously acting as UV absorbers and luminescent downshifting (LDS) layers (Van Der Ende et al., 2009; Huang et al., 2013; Bünzli and Chauvin, 2014; Ferreira et al., 2020). While acting as UV filters, LDS layers do not necessarily decrease the overall efficiency of solar cells because the loss in photocurrent due to the lost UV absorption can be compensated or even exceeded by the current generated upon absorption of photons reemitted by the LDS, with wavelengths matching the range of larger spectral response of the cells. Such an approach has already been used to enhance the response of perovskite-based PV cells in the low-yield UV region while preventing UV-induced PV degradation (Chen et al., 2017; Kim et al., 2017; Rahman et al., 2019). In this regard, an increase in PCE of 14.15% in combination with improved device stability upon incorporating a layer of a Eu^{3+}-based blend at the interface with the perovskite absorbing layer inside the device was reported (Rahman et al., 2019). Recently, some of us used Eu^{3+}- and Tb^{3+}-doped organic–inorganic hybrids as LDS coatings on the top of c-Si-based PV cells and obtained an absolute increase of the external quantum efficiency (EQE) of ~27% in the 300–400 nm spectral region (Correia et al., 2019). In another work, a combined approach using Eu^{3+}-based materials as an LDS layer and luminescent solar concentrator as a single device resulted in a significant increase in the PV cell EQE, of ~32% between 300 and 360 nm relative to the bare PV cell (Cardoso et al., 2020).

Despite the potential of LDS coatings, in the OPVs field, only a few works reported their use to improve PV performance and they refer to solar cells with BHJs containing fullerenes as the acceptor (Wang et al., 2011; Engmann et al., 2012; Das and Narayan, 2013; Ma et al., 2013; Moudam et al., 2015; Fernandes et al., 2017). Organic LDS layers with a UV absorber triphenyl-diamine derivative (TPD) deposited on the transparent side of P3HT:$PC_{61}BM$-based cells caused an increment of 7.2% in PCE after optimizing the TPD layer thickness and covering with an antireflecting LiF layer to trap the emission into the device (Wang et al., 2011). A similar increment in PCE (7.4%) accompanied by improved performance stability was reported for inverted solar cells with the same BHJ, upon using an energy transfer system based on a mixture of the luminescent dyes Kremer Blue and Alq3 dispersed in poly(methyl methacrylate) (Fernandes et al., 2017). As the increment in PCE was mainly due to an increase in the FF and no major impact was observed in the EQE spectrum, the authors hypothesized that the LDS layer modifies the solar radiation power incident on the cell and consequently affects the FF value. These authors also highlighted that the use of a commercial filter instead, as needed for encapsulating the devices for commercial applications, would cause a ~20% drop in PCE due to increased reflection. A higher increment on PCE of 14% for similar devices with P3HT:$PC_{61}BM$ was demonstrated through the use of a titanium and silicon oxide UV-blocking layer in combination with a LDS layer composed of an anthracene derivative dispersed in an epoxy matrix covering the transparent

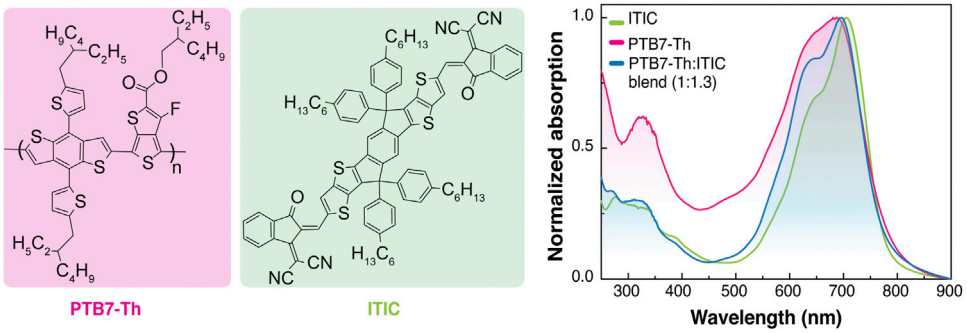

FIGURE 1 | Chemical structure and absorption spectra of the components in the BHJ layer of the studied OPV cells (PTB7-Th and ITIC) as spin-cast films.

side of the solar cells (Engmann et al., 2012). A higher improvement in PCE for P3HT:PC_{61}BM-based cells, of 15%, was shown upon introducing an LDS layer combining two fluorescent molecules, Coumarin 545T and Alq3, in between the indium tin oxide (ITO) electrode and the BHJ layer in inverted cells (Ma et al., 2013). Noteworthy, in these cells, the improvement was related to an EQE enhancement, particularly in the shorter-wavelength region, consistent with the absorption of the Alq3 dye. Other studies focused on solar cells with BHJs with the polymers PCPDTBT or PTB7 as donors and the fullerene acceptor PC_{71}BM (Das and Narayan, 2013; Moudam et al., 2015). In one of such works, downshifting was achieved within the visible, from the 500–600 nm range to the 600–800 nm, this being the spectral range of higher absorption of the BHJ, by using an organic fluorophore termed as 759 Dye dispersed in a dielectric polymer matrix. An enhancement in EQE at wavelengths corresponding to that of the dye absorption was consistent with the observed increase in J_{SC} of about 12% (Das and Narayan, 2013). In another work, the PCE was increased from 3.66 to 3.76% upon introducing an LDS layer based on a UV-absorbing silver(I) complex in PTB7:PC_{71}BM-based solar cells, which was attributed to an EQE enhancement in the UV spectral region (Moudam et al., 2015).

To the best of our knowledge, the application of LDS layers on OPV cells with efficient NFAs has not yet been reported. In this work, we investigate the effect of a di-ureasil organic–inorganic hybrid modified with Eu^{3+} (dU6Eu) LDS layer when applied over the light-incident surface of OPV cells of such a class, namely, with the PTB7-Th:ITIC BHJ (PTB7-Th:poly ([2,6′-4,8-di (5-ethylhexylthienyl)benzo [1,2-b; 3,3-b]dithiophene], also known as PCE-10, ITIC: 3,9-bis(2-methylene-(3-(1,1-dicyanomethylene)-indanone))-5,5,11,11-tetrakis (4-hexylphenyl)-dithieno [2,3-d:2′,3′-d′]-s-indaceno [1,2-b:5,6-b′] dithiophene) (**Figure 1**). The choice of such polymer and acceptor was based on their commercial availability and on their well-documented good performance in their own categories. The OPV cells were fabricated with direct architecture and with the organic layer spin-coated over the hole transport layer (HTL) of LDS/glass/cathode/HTL substrates, yielding semitransparent bluish sets for devices. Analogous devices without the LDS layer were also prepared and tested as control devices. As shown in **Figure 1**, both PTB7-Th and ITIC have intense absorption bands spanning between 500 and 800 nm, while a decrease in the absorption is observed in the UV-blue (up to 400 nm). The rationale behind the LDS layer selection lies in the fact that it presents absorption in the lower wavelength harvesting spectral region (<400 nm) of the BHJ layer and emission in its higher spectral response region (570–710 nm). Thus, by adding an LDS layer with absorption complementary to that of the active PV material and emission matching its maximum spectral response, UV photons that would not be efficiently used by the bare solar cell are now being converted to visible ones, which will be absorbed by the solar cell active layer, increasing the number of available visible photons for PV conversion. A beta-diketonate complex of Eu^{3+}, Eu $(tta)_3{\cdot}2H_2O$, absorbing in the UV region and able to downshift toward the redder part of the spectrum, was selected as an optically active center (**Supplementary Figures S1–S3** in the **Supplementary Material**). This was dispersed in an organic–inorganic hybrid matrix, which presents the advantage of easy processing at room temperature with the desired shape and thickness, due to combining the flexibility of the organic counterpart with the mechanical stability of the inorganic one (Sanchez et al., 2003; Parola et al., 2017; Ramalho et al., 2020). Previous studies pointed out the role of hybrid matrices in improving the photostability of beta-diketonate complexes (Lima et al., 2006; Lima et al., 2013; Ramalho et al., 2020). Moreover, recently, it was reported their stability upon severe accelerated aging tests performed under controlled relative humidity (RH) and temperature, revealing minor changes in the emission quantum yield values. The stability of the emission color was also studied after prolonged continuous solar irradiation (AM1.5G, 1000 Wm^{-2}), revealing that the red emission remained unchanged (Ramalho et al., 2020). Noteworthy, the red emission of the Eu^{3+} complex permits the hybrids to keep their transparency under daylight illumination (negligible absorption in the visible spectral range) (Correia et al., 2018; Correia et al., 2019; Ramalho et al., 2020), since the intense red color can only be seen under UV irradiation. The UV component (300–400 nm) corresponds to a small fraction (~6%) of the AM1.5G solar spectrum; thus, the transparency of the device is not compromised (Correia et al., 2018; Correia et al., 2019). Furthermore, the Eu $(tta)_3.2H_2O$ complex was chosen because after incorporation into the hybrid host, the water molecules coordinated to the Eu^{3+} ions are replaced with the oxygen

atoms from the carbonyl groups of the urea cross-linkages, contributing to a remarkable increase in the absolute emission quantum yield (q, defined as the ratio between the number of emitted and absorbed photons), from 0.27 (for the isolated complex) to 0.80 (dU6Eu) (Correia et al., 2016). Noteworthy, hybrid matrices incorporating this complex were already used for silicon-based PV applications as optically active layers in luminescent solar concentrators (Correia et al., 2015; Correia et al., 2016; Correia et al., 2018) and as LDS layers (Correia et al., 2019). In terms of photophysical characteristics, the selected luminescent material also presents optimal features for LDS applications: 1) high absorption coefficient that translates into an effective ability to harvest solar photons in the absorption spectral range (overlap integral, *O*, between the absorption spectra and the AM1.5G spectrum, corresponds to ca. 1.5% of the total solar photons available on earth); high q values (0.85 ± 0.08) (Correia et al., 2016); 3) large ligands-induced Stokes shift that prevents self-absorption, 4) high thermal stability (Correia et al., 2015; Correia et al., 2016; Correia et al., 2018; Correia et al., 2019; Ramalho et al., 2020). Finally, their siliceous-based gel formulation and air-stability enable easy processing from solutions using benign solvents (ethanol), convenient for large-scale applications (Ramalho et al., 2020).

EXPERIMENTAL DETAILS

Materials and Methods

All the solvents and reagents were purchased from commercial sources and used without further purification. The PEDOT-PSS (poly(3,4-ethylenedioxythiophene)-poly(styrenesulfonate)) as water dispersion was acquired from Heraeus (CLEVIOS™ PVP AI 4083). PTB7-Th and ITIC were purchased from Ossila. The nonhydrolyzed organic–inorganic hybrid precursor, d-UPTES (600) (**Supplementary Figure S1A** in the **Supplementary Material**), was prepared according to the literature (supplementary data for details). The Eu $(tta)_3{\cdot}2H_2O$ complex (**Supplementary Figure S1B** in the **Supplementary Material**) was synthesized by the reaction of europium chloride ($EuCl_3{\cdot}6H_2O$, Sigma-Aldrich, 99%) and 2-thenoyltrifluoroacetone (tta, Sigma-Aldrich) in the presence of NaOH (Merck, 98%) ethanol (EtOH, Fisher Scientific) solution as fully described elsewhere (supplementary data). The Eu^{3+}-doped d-U (600) solution was prepared by dissolving the Eu $(tta)_3.2H_2O$ complex in ethanol (HPLC grade) and adding the solution to the d-UPTES (600) with magnetic stirring until a homogeneous solution is formed. For this, 17 mg of Eu $(tta)_3.2H_2O$ was dissolved in 0.82 ml of ethanol and the solution was added to 1.91 g of d-U (600), resulting in an Eu $(tta)_3.2H_2O$/d-U (600) wt% of 0.89% (C1). Then, HClaq. 1 M was added (6.7% with respect to the ethanol) and the solution was stirred for *ca.* 30 s to produce a gel-like solution. The Eu^{3+}-doped di-ureasil will be hereafter termed as dU6Eu.

UV–Vis absorption spectra were determined using a Cecil 7,200 spectrophotometer or a Lambda 950 dual-beam spectrometer (PerkinElmer). The photoluminescence spectra were recorded with a modular double-grating excitation spectrofluorometer with a TRIAX 320 emission monochromator (Fluorolog-3, Horiba Scientific) and a spectrofluorometer (FluoroMax-4, Horiba Scientific) equipped with a monochromator, both coupled to a R928 Hamamatsu photomultiplier. The emission decay curves were measured with the setup described for the luminescence spectra using a pulsed Xe–Hg lamp (6 μs pulse at half-width and 20–30 μs tail). The absolute emission quantum yield (q) values were measured at room temperature using a C9920–02 Hamamatsu system. The method is accurate within 10%. The thicknesses of the LDS layers were determined using a Dektak profilometer. Atomic force microscopy (AFM) measurements were performed on a Nano Observer microscope from Concept Scientific Instruments (Les Ulis, France) in noncontact mode. Cantilevers with a resonance frequency between 200 and 400 kHz and silicon probes with tip radius smaller than 10 nm from AppNano were used. All images were taken at a resolution of 256 × 256 pixels and were processed with Gwyddion (version 2.26) software. In this study, all measurements of device performance were performed under N_2 atmosphere to eliminate possible effects related to extrinsic factors as oxygen and moisture in the ambient.

Devices Fabrication and Characterization

The OPV cells were fabricated according to the scheme in **Figure 2** with the structure glass/ITO/PEDOT:PSS/PTB7-Th:ITIC/Ca (20 nm)/Al (80 nm) (control devices) and with the LDS layer prior to the glass exterior surface.

Glass/ITO substrates were first cleaned with a nonionic detergent, distilled water, acetone (HPLC grade), and 2-propanol (HPLC grade) successively under ultrasounds. The substrates were then dried with N_2 flow and subjected to UV-oxygen plasma for 3 min prior to the deposition of a *ca.* 40 nm thick layer of PEDOT:PSS by spin-coating (1800 rpm for 45 s, at room temperature, using a Chemat Technology KW-4A spin coater). The substrates were then dried at 125°C for 10 min in air. The glass/ITO/PEDOT:PSS substrates were placed on microscope slides with the PEDOT:PSS facing downwards, and the Scotch tape was placed at the edges sealing them with the slides to prevent the leakage of LDS solution into the device during its deposition. The LDS layer was then spin-coated at 500/1,000 rpm for 15/45 s or drop-cast on top of the upper face of the substrates under air conditions and left under air for 24 h at room temperature for cross-linking reactions to occur. The dU6Eu is then obtained as a rigid and glassy layer. Afterward, the substrates were released from the slides and transferred to a N_2-filled glovebox to deposit the PTB7-Th:ITIC blend solution. This was prepared with 15 mg/ml in concentration with a 1:1.3 polymer:acceptor mass proportion in chlorobenzene. The blend solution was stirred overnight at 100°C and spin-coated (1,300 rpm for 60 s) while hot over the PEDOT:PSS layer surface. Finally, the resulting substrates were transferred to a high-vacuum chamber inside the glovebox with a base pressure of 2×10^{-6} mbar to evaporate a 20 nm thick Ca layer followed by a 60–100 nm thick Al through a shadow mask, defining the active device area of 0.24 cm^2 (as determined by the overlap of ITO and Ca/Al electrodes). At least 8 devices were prepared for each condition. In all the device fabrication processes, an analogous

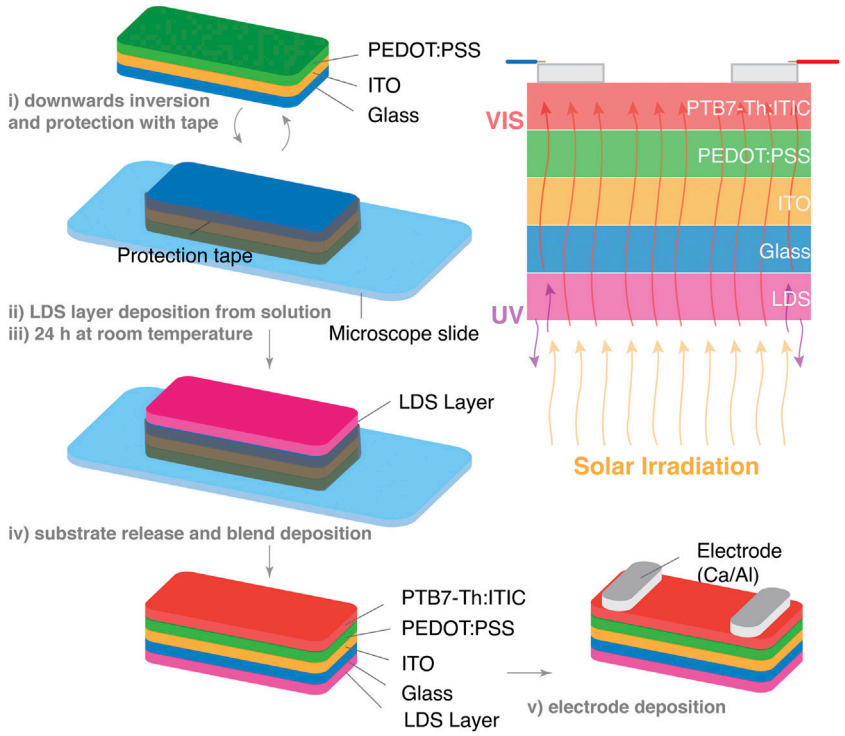

FIGURE 2 | Outline of the fabrication steps of the dU6Eu LDS-coated OPV devices in this study and depiction of the UV-filtering and light downshifting phenomena taking place in the LDS layer.

set of control devices, i.e., without LDS layer, was meticulously prepared under the same conditions except that the LDS coating was not deposited.

The current-voltage (*J–V*) characteristics of the devices were measured at room temperature using a solar simulator (Newport, Oriel Sol 3A, 69,920) with 1000 W/m^2 AM1.5G output (calibrated with a silicon reference solar cell from Oriel) and a Keithley 2,400 Source-Meter for current-voltage measurements. The devices were mounted under N_2 into a measurement chamber and kept under an inert atmosphere during the measurements. The EQE spectra were determined at short-circuit conditions using monochromatic light from a homemade setup with a xenon lamp as light source.

RESULTS AND DISCUSSION

The LDS layers were integrated into the cells following the steps depicted in **Figure 2** as spin-coated or drop-cast layers (as described in the experimental section). In addition, a twofold concentration (2×C1) of the Eu $(tta)_3.2H_2O$ complex in the hybrid matrix was tested to determine the effect of the density of optically active centers in the LDS layer. Also, a different set of cells was fabricated with coatings prepared without the complex, i.e., consisting solely of the nondoped di-ureasil host, d-U (600). For all the sets of fabricated devices with the LDS layer, a parallel set of control devices (without LDS layer) was prepared with the same blend solution and meticulously replicating all the fabrication steps (where the Ca/Al electrode was simultaneously evaporated over the two sets). This allows for fair comparisons with control devices and minimizes errors associated with the relatively large dispersity of PCE values found from batch to batch. These dissimilarities in performance parameters are probably related to small differences in the polymer:ITIC ratio and/or with the thickness of the BHJ layer and are also found in the literature for devices prepared under the same conditions (Song et al., 2017; Doumon et al., 2019; Gurnay et al., 2019; Wang et al., 2019).

Figure 3 depicts the room-temperature excitation and emission spectra of the dU6Eu and the EQE curves obtained for all the devices prepared with and without the LDS layers (control devices) and **Figure 4** shows the J-V characteristics obtained for the cells containing the less doped spin-coated dU6Eu LDS ($[Eu^{3+}]$ = 0.89% (C1)) layers deposited by spin-coating, for which a significant enhancement (ca. 22%) in PCE was obtained upon integrating dU6Eu as LDS layer.

As shown in **Table 1**, for the remaining studied cases, no significant variations in the averaged performance parameters were found, where the variations in the devices' performance were determined as the relative increment of the average values over those of the control devices (e.g., $\Delta J_{SC}/J_{sc}$ (%) = 100× (J_{SC}, average for cells with LDS–*J*SC, average for control cells)/ $J_{SC,\ \text{average for control cells}}$), measured under AM1.5G illumination.

As **Figure 3A** shows, the spectral characteristics of the dU6Eu LDS coatings allow for anticipating UV/blue filtering in combination with downshifting to spectral regions where the

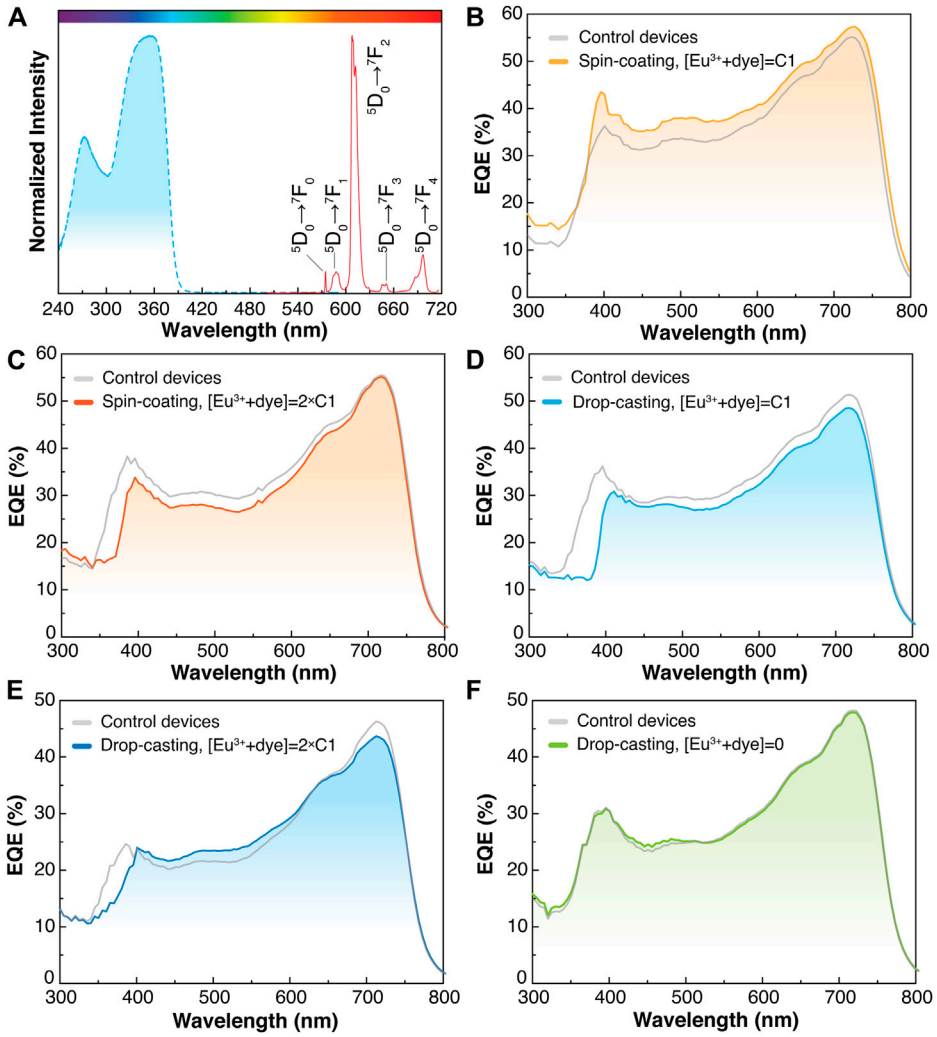

FIGURE 3 | (A) Excitation (dashed line) and emission (solid line) spectra of dU6Eu monitored at 612 nm and excited at 365 nm, respectively. **(B–F)** EQE spectra of the dU6Eu/glass/ITO/PEDOT:PSS/PTB7-Th:ITIC/Ca/Al devices prepared in this study and comparison with those of the control devices.

studied cells present higher yield spectral response. In particular, the emission spectrum is composed of the typical Eu^{3+} $^5D_0 \rightarrow {}^7F_{0-4}$ transitions. The absence of ligands and hybrids intrinsic emission indicates effective energy transfer to the Eu^{3+} ions, as demonstrated in the excitation spectra that reveal three main components, peaking at 270, 320, and 365 nm, mainly ascribed to the hybrid host (Freitas et al., 2013) and to the tta excited states (Molina et al., 2003; Nolasco et al., 2013), respectively. The 320 and 365 nm components resemble those already observed for isolated $Eu(tta)_3{\cdot}2H_2O$ (Kai et al., 2011) and for organic–inorganic hybrids incorporating Eu^{3+} complexes, being ascribed to the π-π* electronic transition of the organic ligands (Fernandes et al., 2007). Apart from changes in the relative intensity, the UV-visible absorption spectrum reveals the same components detected in excitation spectra (**Supplementary Figure S4** in the **Supplementary Material**). We should note that the modifications in the processing routine (relative to previously reported ones in order to control viscosity and deposition methods) did not induce any significant changes in the optical features of the material (**Supplementary Figure S2** in the **Supplementary Material**) (Correia et al., 2015; Correia et al., 2016; Correia et al., 2018; Ramalho et al., 2020). Minor changes in the energy and relative intensity were previously assigned to the solvent evaporation rate (Pecoraro et al., 2008; Graffion et al., 2011; Correia et al., 2020). Nevertheless, the Eu^{3+} local coordination remains the same as the energy of the $^5D_0 \rightarrow {}^7F_{0-4}$ transitions and analogous $^5D_0$ lifetime values were measured (Ramalho et al., 2020), independently of the processing (**Supplementary Figure S2** in the **Supplementary Material**). The light-harvesting ability of the dU6Eu LDS layers was evaluated through the estimation of the overlap integral O between the absorbance and the sunlight available for PV conversion (see **Supplementary Material** for details) (Reisfeld et al., 1994; Rondão et al., 2017). A value of $O = 4.5 \times 10^{19}$ photons $s^{-1}m^{-2}$ was found (**Supplementary Figure S4** in the **Supplementary Material**), indicating that these LDS coatings

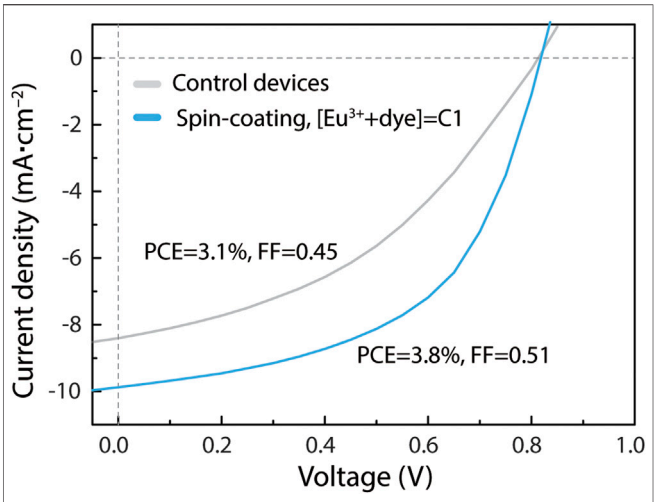

FIGURE 4 | J-V characteristics of dU6Eu/glass/ITO/PEDOT:PSS/PTB7-Th:ITIC/Ca/Al devices for which an improvement in PCE of ca. 22% was obtained in comparison with control devices.

have the potential to absorb ~1.1% of the solar photon flux on the earth surface (4.3×10^{21} photons s^{-1} m^{-2}) (Bünzli and Chauvin, 2014), similar to the values found in previous studies for analogous materials (Correia et al., 2019).

As observed in **Table 1** and **Figure 4**, the most improved cells, revealing a remarkable enhancement of 22% in the average PCE (the average PCE is raised from 3.1 to 3.8%), showed enhancements of 7 and 13% in J_{SC} and FF values, respectively, while V_{OC} was not affected.

A small improvement in PCE, of 2%, was also obtained for the cells with LDS layers deposited by drop-casting with a twofold concentration of Eu^{3+} centers, although the error indicates that the variation may be less or even negative (**Table 1**). The EQE spectrum of the most improved cells (**Figure 3B**) shows an enhancement of ~29%, at the 300–360 nm range, which corresponds to the absorption spectral region of the LDS layer, as shown in **Figure 3A**, indicating that, even with an absolute emission quantum yield below the unit, the number of available photons is higher than that in the case of the bare solar cell. In addition, the EQE values are increased in most of the spectrum, indicating that the LDS layer is causing an overall beneficial effect on the cells. In what concerns the EQE spectra of all the OPV devices, the rising edge at higher energies of the EQE band is red-shifted in relation to those of the control cells, except in those in which the LDS layer does not contain the Eu^{3+} complex (**Figure 3F**). Such redshifts match well to the excitation/absorption edge of the LDS layer (**Figure 3A** and **Supplementary Figure S4** in the **Supplementary Material**) and therefore are consistent with the occurrence of UV-blue filtering caused by the LDS layer. The absence of redshift in the EQE of the cells with LDS lacking the optically active centers indicates that the Eu^{3+} complex ligands are the main absorbers contributing to the UV-blue filtering while the contribution of the bare matrix is practically negligible. The slightly negatively affected performance (considering the averaged values) of the cells with nondoped LDS, d-U (600), is probably due to a minor UV-filtering effect ascribed to the low absorption of the bare matrix (**Supplementary Figure S5** in the **Supplementary Material**). Thus, we suggest that the two effects, UV-filtering and the emission downshifting, are present in the cells with the LDS layers, although their contributions to the cells' performance vary in accordance with the LDS features. For the cells showing an average improvement in PCE of 22%, the enhancement of the EQE in the UV region can be interpreted as a result of a balance between photogenerated charges associated with LDS photon conversion and photon loss due to UV-filtering at the LDS layer, where the first surpasses the latter. The improvement of ~13% in the FF values found for the same cells should be related to a benefit on the blend properties caused by the reduction in UV radiation hitting the cell. This might explain the EQE increase in the spectral range where the LDS layer has no absorption and is in accordance with other studies showing the positive effect of UV-filtering in the FF (Fernandes et al., 2017; Doumon et al., 2019).

In order to investigate eventual differences between the BHJ blends in the devices coated with the LDS layers and those in noncoated cells that could be related to the benefit attributed to the UV-filtering effect (e.g., differences in morphologies that could affect charge carriers mobilities), we performed AFM analysis on the BHJ blends before and after illumination of the cells. However, no noticeable modifications were found (**Supplementary Figure S6** in the **Supplementary Material**), although the blend films in the LDS-coated cells get a little smoother upon illumination than those in noncoated cells. Still, it should be noted that modifications on the BHJ at the inner scale cannot be perceived by AFM. Further studies to unravel the origin of the benefitting effect of UV-filtering in these cells will focus on the intrinsic photodegradation of the active components and on the effects of UV illumination on the

TABLE 1 | Relative variations in performance parameters of glass/ITO/PEDOT:PSS/PTB7-Th:ITIC/CA/Al devices with dU6Eu LDS layers deposited under different conditions in comparison with control devices without LDS.

LDS layer	V_{oc}(V)	$\Delta J_{sc}/J_{sc}$ (%)	ΔFF/FF (%)	ΔPCE/PCE (%)
Spin-coated, [Eu^{3+}] = C1[a]	0.81	7 ± 6	13 ± 5	22 ± 7
Spin-coated, [Eu^{3+}] = 2×C1	0.80	−1 ± 2	0 ± 3	−1 ± 3
Drop-cast, [Eu^{3+}] = C1	0.81	−3 ± 7	−1 ± 5	−4 ± 7
Drop-cast, [Eu^{3+}] = 2×C1	0.81	0 ± 2	2 ± 4	2 ± 4
Drop-cast, [Eu^{3+}] = 0[b]	0.81	−1 ± 5	−1 ± 3	−2 ± 6

[a]*C1 = ($m_{Eu}/m_{d\text{-}U(600)}$) = 0.89%.*
[b]*The LDS layer is pristine d-U (600).*

photophysical processes taking place in the active blends during their operation.

Regarding the cells with spin-cast LDS layers with the twofold concentration of the Eu^{3+} complex, their EQE spectra (**Figure 3C**) exhibit pronounced redshifts of the rising edge of the band at higher energies, indicating a strong UV-blue filtering effect. To interpret this effect, we tested the hypothesis of aggregates formation in the doubly concentrated LDS samples that could degrade their optical properties and reduce the LDS efficiency. Thus, the excitation and emission spectra and emission decay curves of the LDS layers containing the dU6Eu in both concentrations of Eu^{3+} complex (**Supplementary Figures S7, S8** in the **Supplementary Material**) were measured. However, analogous spectral profiles for both samples were obtained, thus indicating that the twofold increase in the complex concentration does not induce significant changes in the local coordination of the lanthanide ions, thus supporting the absence of aggregates or clusters. Moreover, concentration quenching effects are also ruled out as the $^5D_0$ lifetime value is also independent of the concentration in the studied range. Since analogous radiative transition probability can be inferred from the similarity of the emission spectra, the same lifetime value indicates analogous nonradiative transition probability. Hence, it can be concluded that the more pronounced redshift in the EQE of the cells with twofold concentration of Eu^{3+}-complex can be tentatively attributed to the increase in absorbing centers in the LDS layers.

The effect of the LDS thickness on the EQE spectra can be observed by comparing the cells with spin-coated LDS layers (thickness = 24 ± 1 μm) and those with LDS layers deposited by drop-casting (thickness = 47 ± 2 μm). For the cells with less doped LDS layers, i.e., [Eu^{3+} complex] = C1, the EQE spectra of the cells coated with the thick LDS layers (**Figure 3D**) show more pronounced redshifts. Such loss in EQE is in accordance with the obtained decrease in the performance of such cells (entry 3 in **Table 1**) and is likely due to an unbalance between photogenerated charges upon LDS and photon loss from UV-filtering effect at the LDS layer, the latter being more intense. However, for the cells with LDS layers with a twofold concentration of Eu^{3+} complex, similar pronounced redshifts are observed in both types of cells (with thin and thick LDS layers), which are probably due to a strong UV-filtering effect associated with the high concentration of absorbing centers in both types of LDS layers.

CONCLUSION

In this work, the PCE of organic solar cells based on the PTB7-Th: ITIC blend was significantly increased (22%) by introducing a luminescent layer based on Eu^{3+}-modified di-ureasil organic–inorganic hybrids on top of the transparent side of the cells. The improvement of such devices was attributed to the UV LDS effect that compensates for the photocurrent loss caused by the absorption of UV photons together with a benefitting UV-filtering effect on the cells. The latter can possibly reduce intrinsic photodegradation of the active blend; however, further studies are needed to unravel the precise mechanisms caused by UV filtering. It was found that the increase in both the LDS thickness and the concentration of optically active centers increases the UV absorption and can lead to a major decrease in the photocurrent generated on that spectral region. The luminescent layers described in this work, composed of a Eu^{3+} complex dispersed in an organic–inorganic hybrid matrix, can be easily deposited by solution deposition methods as roll-to-roll printing using benign solvents (ethanol), and therefore they represent interesting coatings for future applications in large-area devices.

DATA AVAILABILITY STATEMENT

The original contributions presented in the study are included in the article/**Supplementary Material**; further inquiries can be directed to the corresponding authors.

AUTHOR CONTRIBUTIONS

All authors contributed to this work. SC and LF performed the synthesis of the hybrid precursor and of the complex. JF and AC performed the hybrids gelification and the OPV development. SC and AB performed the photoluminescence characterization. JF and AC carried out the electrical measurements. SC, AB, RF, and PA analyzed all the photoluminescence results, while AC, JF, and PA discussed the electrical measures. AC, RF, and PA wrote the draft of the manuscript, while all the remaining authors provided critical feedback and helped with the analysis and writing process of the manuscript. All the authors discussed the results and implications and commented on the manuscript at all stages.

FUNDING

This work was developed within the scope of the projects at CICECO-Aveiro Institute of Materials (UIDB/50011/2020&UIDP/50011/2020), Instituto de Telecomunicações (UIDB/50008/2020-UIDP/50008/2020), the projects Solar-Flex (CENTRO-01–0145-FEDER-030186), SusPhotoSolutions (CENTRO-01–0145-FEDER-000005), and Suprasol (PTDC/QUI-QOR/28365/2017) financed by national funds through the FCT/MEC, and when appropriate cofinanced by FEDER under the PT2020 Partnership Agreement through European Regional Development Fund (ERDF) in the frame of Operational Competitiveness and Internationalization Program (POCI).

ACKNOWLEDGMENTS

LF acknowledges WINLEDs (POCI-01–0145-FEDER-030351).

SUPPLEMENTARY MATERIAL

The Supplementary Material for this article can be found online at: https://www.frontiersin.org/articles/10.3389/fnano.2021.635929/full#supplementary-material.

REFERENCES

Bünzli, J. C. G., and Chauvin, A. S. (2014). "Lanthanides in solar energy conversion," in *Handbook on the physics and chemistry or Rare earths*. Editor B. V. Elsevier (Amsterdam, Netherlands: Imprint), 480.

Cardoso, M. A., Correia, S. F. H., Frias, A. R., Gonçalves, H. M. R., Pereira, R. F. P., Nunes, S. C., et al. (2020). Solar spectral conversion based on plastic films of lanthanide-doped ionosilicas for photovoltaics: down-shifting layers and luminescent solar concentrators. *J. Rare Earths.* 38, 531–538. doi:10.1016/j.jre.2020.01.007

Cha, H., Wu, J., Wadsworth, A., Nagitta, J., Limbu, S., Pont, S., et al. (2017). An efficient, "burn in" free organic solar cell employing a nonfullerene electron acceptor. *J. Adv. Mater.* 29, 1701156. doi:10.1002/adma.201701156

Chen, W., Luo, Q., Zhang, C., Shi, J., Deng, X., Yue, L., et al. (2017). Effects of down-conversion CeO2:Eu^{3+} nanophosphors in perovskite solar cells. *J. Mater. Sci. Mater. Electron.* 28, 11346–11357. doi:10.1007/s10854-017-6928-0

Correia, S. F. H., Lima, P. P., André, P. S., Ferreira, R. A. S., and Carlos, L. D. (2015). High-efficiency luminescent solar concentrators for flexible waveguiding photovoltaics. *Sol. Energ. Mater. Sol. Cells* 138, 51–57. doi:10.1016/j.solmat.2015.02.032

Correia, S. F. H., Lima, P. P., Pecoraro, E., Ribeiro, S. J. L., André, P. S., Ferreira, R. A. S., et al. (2016). Scale up the collection area of luminescent solar concentrators towards metre-length flexible waveguiding photovoltaics. *Prog. Photovolt Res. Appl.* 24, 1178–1193. doi:10.1002/pip.2772

Correia, S. F. H., Frias, A. R., Fu, L., Rondão, R., Pecoraro, E., Ribeiro, S. J. L., et al. (2018). Large-area tunable visible-to-near-infrared luminescent solar concentrators. *Adv. Sustain. Syst.* 2, 1800002. doi:10.1002/adsu.201800002

Correia, S. F. H., Bastos, A. R. N., Fu, F., Carlos, L. D., André, P. S., and Ferreira, R. A. S. (2019). Lzanthanide-based downshifting layers tested in a solar car race. *Opto Electron. Adv.* 2, 190006. doi:10.29026/0ea.2019.190006

Correia, S. F. H., Fernandes, R. L., Fu, L., Nolasco, M. M., Carlos, L. D., and Ferreira, R. A. S. (2020). High emission quantum yield Tb^{3+} -activated organic-inorganic hybrids for UV-Down-Shifting green light-emitting diodes. *Eur. J. Inorg. Chem.* 2020, 1736–1742. doi:10.1002/ejic.202000054

Das, A. J., and Narayan, K. S. (2013). Retention of power conversion efficiency–from small area to large area polymer solar cells. *J. Adv. Mater.* 25, 2193–2199. doi:10.1002/adma.201204048

Distler, A., Sauermann, T., Egelhaaf, H.-J., Rodman, S., Walker, D., Cheon, K.-S., et al. (2014). The effect of PCBM dimerization on the performance of bulk heterojunction solar cells. *Adv. Energ. Mater.* 4, 1300693. doi:10.1002/aenm.201300693

Doumon, N. Y., Dryzhov, M. V., Houard, F. V., Le Corre, V. M., Chatri, A. R., Christodoulis, P., et al. (2019). Photostability of fullerene and non-fullerene polymer solar cells: the role of the acceptor. *ACS Appl. Mater. Inter.* 11, 8310–8318. doi:10.1021/acsami.8b20493

Engmann, S., Machalett, M., Turkovic, V., Rösch, R., Rädlein, E., Gobsch, G., et al. (2012). Photon recycling across a ultraviolet-blocking layer by luminescence in polymer solar cells. *J. Appl. Phys.* 112, 034517. doi:10.1063/1.4745016

Fernandes, M., de Zea Bermudez, V., Ferreira, R. A. S., Carlos, L. D., Charas, A., Morgado, J., et al. (2007). Highly photostable luminescent poly(ε-caprolactone) siloxane biohybrids doped with europium complexes. *Chem. Mater.* 19, 3892–3901. doi:10.1021/cm062832n

Fernandes, R. V., Bristow, N., Stoichkov, V., Anizelli, H. S., Duarte, J. L., Laureto, E., et al. (2017). Development of multidye UV filters for OPVs using luminescent materials. *J. Phys. D: Appl. Phys.* 50, 025103. doi:10.1088/1361-6463/50/2/025103

Ferreira, R. A. S., Correia, S. F. H., Monguzzi, A., Liu, X., and Meinardi, F. (2020). Spectral converters for photovoltaics–what's ahead. *Mater. Today* 33, 105–121. doi:10.1016/j.mattod.2019.10.002

Freitas, V. T., Lima, P. P., Ferreira, R. A. S., Pecoraro, E., Fernandes, M., de Zea Bermudez, V., et al. (2013). Luminescent urea cross-linked tripodal siloxane-based hybrids. *J. Sol. Gel. Sci. Technol.* 65, 83–92. doi:10.1007/s10971-012-2770-2

Graffion, J., Cattoën, X., Man, M. W. C., Fernandes, V. R., André, P. S., Ferreira, R. A. S., et al. (2011). Modulating the photoluminescence of bridged silsesquioxanes incorporating Eu^{3+}-Complexedn,n′-Diureido-2,2′-bipyridine isomers: application for luminescent solar concentrators. *Chem. Mater.* 23, 4773–4782. doi:10.1021/cm2019026

Gurnay, R. S., Li, W., Yan, Y., Liu, D., Pearson, A. J., and Wang, T. (2019). Morphology and efficiency enhancements of PTB7-Th:ITIC nonfullerene organic solar cells processed via solvent vapor annealing. *J. Energ. Chem.* 37, 148–156. doi:10.1016/j.jechem.2018.12.015

Heumueller, T., Mateker, W. R., Sachs-Quintana, I. T., Vandewal, K., Bartelt, J. A., Burke, T. M., et al. (2014). Reducing burn-in voltage loss in polymer solar cells by increasing the polymer crystallinity. *Energ. Environ. Sci.* 7, 2974–2980. doi:10.1039/c4ee01842g

Heumueller, T., Burke, T. M., Mateker, W. R., Sachs-Quintana, I. T., Vandewall, K., Brabec, C. J., et al. (2015). Disorder-induced open-circuit voltage losses in organic solar cells during photoinduced burn-in. *Adv. Energ. Mater.* 5, 1500111. doi:10.1002/aenm.201500111

Heumueller, T., Mateker, W. R., Distler, A., Fritze, U. F., Cheacharoen, R., Nguyen, W. H., et al. (2016). Morphological and electrical control of fullerene dimerization determines organic photovoltaic stability. *Energy Environ. Sci.* 9, 247–256. doi:10.1039/c5ee02912k

Huang, X., Han, S., Huang, W., and Liu, X. (2013). Enhancing solar cell efficiency: the search for luminescent materials as spectral converters. *Chem. Soc. Rev.* 42, 173–201. doi:10.1039/c2cs35288e

Kai, J., Felinto, M. C. F. C., Nunes, L. A. O., Malta, O. L., and Brito, H. F. H. F. (2011). Intermolecular energy transfer and photostability of luminescence-tuneable multicolour PMMA films doped with lanthanide-β-diketonate complexes. *J. Mater. Chem.* 21, 3796–3802. doi:10.1039/c0jm03474f

Kim, C. W., Eom, T. Y., Yang, I. S., Kim, B. S., Lee, W. I., Kang, Y. S., et al. (2017). Dual-function Au@Y2O3:Eu^{3+} smart film for enhanced power conversion efficiency and long-term stability of perovskite solar cells. *Sci. Rep.* 7, 6849. doi:10.1038/s41598-017-07218-4

Kong, J., Song, S., Yoo, M., Lee, G. Y., Kwon, O., Park, J. K., et al. (2014). Long-term stable polymer solar cells with significantly reduced burn-in loss. *Nat. Commun.* 5, 5688. doi:10.1038/ncomms6688

Lima, P. P., Ferreira, R. A. S., Freire, R. O., Almeida Paz, F. A., Fu, L., Alves, S., et al. (2006). Spectroscopic study of a UV-photostable organic-inorganic hybrids incorporating an Eu^{3+} beta-diketonate complex. *ChemPhysChem* 7, 735–746. doi:10.1002/cphc.200500588

Lima, P. P., Nolasco, M. M., Paz, F. A. A., Ferreira, R. A. S., Longo, R. L., Malta, O. L., et al. (2013). Photo-click chemistry to design highly efficient lanthanide β-diketonate complexes stable under UV irradiation. *Chem. Mater.* 25, 586–598. doi:10.1021/cm303776x

Lin, Y., Adilbekova, B., Firdaus, Y., Yengel, E., Faber, H., Sajjad, M., et al. (2019). 17% efficient organic solar cells based on liquid exfoliated WS_2 as a replacement for PEDOT:polystyrene sulfonate. *Adv. Mater.* 31, 1902965. doi:10.1002/adma.201902965

Liu, Q., Toudert, J., Mantilla-Perez, P., Bajo, M. M., Russell, T. P., and Martorell, J. (2017). Circumventing UV light induced nanomorphology disorder to achieve long lifetime PTB7-Th:PCBM based solar cells. *Adv. Energ. Mater.* 7, 1701201. doi:10.1002/aenm.201701201

Ma, G.-F., Xie, H.-J., Cheng, P.-P., Li, Y.-Q., and Tang, J.-X. (2013). Performance enhancement of polymer solar cells with luminescent down-shifting sensitizer. *Appl. Phys. Lett.* 103, 043302. doi:10.1063/1.4816383

Mateker, W. R., and Mcgehee, M. D. (2017). Progress in understanding degradation mechanisms and improving stability in organic photovoltaics. *Adv. Mater. Weinheim* 29, 1603940. doi:10.1002/adma.201603940

Molina, C., Dahmouche, K., Messaddeq, Y., Ribeiro, S. J. L., Silva, M. A. P., de Zea Bermudez, V., et al. (2003). Enhanced emission from Eu(III) β-diketone complex combined with ether-type oxygen atoms of di-ureasil organic-inorganic hybrids. *J. Lumin.* 104, 93–101. doi:10.1016/s0022-2313(02)00684-1

Moudam, O., Bristow, N., Chang, S.-W., Horie, M., and Kettle, J. (2015). Application of UV-absorbing silver(I) luminescent down shifter for PTB7 organic solar cells for enhanced efficiency and stability. *RSC. Adv.* 5, 12397–12402. doi:10.1039/c4ra14794d

Nolasco, M. M., Vaz, P. M., Freitas, V. T., Lima, P. P., André, P. S., Ferreira, R. A. S., et al. (2013). Engineering highly efficient Eu(III)-based tri-ureasil hybrids toward luminescent solar concentrators. *J. Mater. Chem.* 1, 7339–7350. doi:10.1039/c3ta11463e

Parola, S., Julián-López, B., Carlos, L. D., and Sanchez, C. (2017). Optical properties of hybrid organic-inorganic materials and their applications - part I: luminescence and photochromism. *J. Solid. State. Chem.* 26, 6506–6554. doi:10.1002/adfm.201602730

Pecoraro, E., Ferreira, R. A. S., Molina, C., Ribeiro, S. J. L., Messsaddeq, Y., and Carlos, L. D. (2008). Photoluminescence of bulks and thin films of Eu^{3+}-doped organic/inorganic hybrids. *J. Alloy. Compd.* 451, 136–139. doi:10.1016/j.jallcom.2007.04.123

Peters, C. H., Sachs-Quintana, I. T., Mateker, W. R., Heumueller, T., Rivnay, J., Noriega, R., et al. (2012). The mechanism of burn-in loss in a high efficiency polymer solar cell. *Adv. Mater. Weinheim* 24, 663–668. doi:10.1002/adma.201103010

Rahman, N. U., Khan, W. U., Khan, S., Chen, X., Khan, J., Zhao, J., et al. (2019). A promising europium-based down conversion material: organic-inorganic perovskite solar cells with high photovoltaic performance and UV-light stability. *J. Mater. Chem. A.* 7, 6467–6474. doi:10.1039/c9ta00551j

Ramalho, J. F. C. B., Correia, S. F. H., Fu, L., Dias, L. M. S., Adão, P., Mateus, P., et al. (2020). Super modules-based active QR codes for smart trackability and IoT: a responsive-banknotes case study. *Npj Flexible Electron* 4, 11. doi:10.1038/s41528-020-0073-1

Reisfeld, R., Shamrakov, D., and Jorgensen, C. (1994). Photostable solar concentrators based on fluorescent glass films. *Sol. Energ. Mater. Sol. Cells* 33, 417–427. doi:10.1016/0927-0248(94)90002-7

Rondão, R., Frias, A. R., Correia, S. F. H., Fu, L., de Zea Bermudez, V., André, P. S., et al. (2017). High-performance near-infrared luminescent solar concentrators. *ACS Appl. Mater. Inter.* 9, 12540–12546. doi:10.1021/acsami.7b02700

Sanchez, C., Lebeau, B., Chaput, F., and Boilot, J.-P. (2003). Optical properties of functional hybrid organic-inorganic nanocomposites. *Funct. Hybrid Mater.* 15, 122–171. doi:10.1002/3527602372.ch5

Song, X., Gasparini, N., and Baran, D. (2017). The influence of solvent additive on polymer solar cells employing fullerene and non-fullerene acceptors. *Adv. Electron. Mater.* 4, 1700358. doi:10.1002/aelm.201700358

Upama, M. B., Wright, M., Mahmud, M. A., Elumalai, N. K., Soufiani, A. M., Wang, D., et al. (2017). Photo-degradation of high efficiency fullerene-free polymer solar cells. *Nanoscale* 9, 18788–18797. doi:10.1039/c7nr06151j

Van Der Ende, B. M., Aarts, L., and Meijerink, A. (2009). Lanthanide ions as spectral converters for solar cells. *Phys. Chem. Chem. Phys.* 11, 11081–11095. doi:10.1039/b913877c

Wang, F., Chen, Z., Xiao, L., Qu, B., and Gong, Q. (2011). Enhancement of the power conversion efficiency by expanding the absorption spectrum with fluorescence layers. *Opt. Express.* 19, A361–A368. doi:10.1364/oe.19.00a361

Wang, X., Yang, Y., He, Z., Wu, H., and Cao, Y. (2019). Influence of the acceptor crystallinity on the open-circuit voltage in PTB7-Th: ITIC organic solar cells. *J. Mater. Chem. C.* 7, 14861–14866. doi:10.1039/c9tc05096e

Xu, H., Yuan, F., Zhou, D., Liao, X., Chen, L., and Chen, Y. (2020). Hole transport layers for organic solar cells: recent progress and prospects. *J. Mater. Chem. A.* 8, 11478–11492. doi:10.1039/d0ta03511d

Conflict of Interest: The authors declare that the research was conducted in the absence of any commercial or financial relationships that could be construed as a potential conflict of interest.